



Decentralized plantwide control strategy for large-scale processes. Case study: Pulp mill benchmark problem



P.A. Luppi ^{a,b}, D.A.R. Zumoffen ^{a,c}, M.S. Basualdo ^{a,c,b,*}

^a Computer Aided Process Engineering Group (CAPEG), French Argentine International Center for Information and Systems Sciences (CIFASIS – CONICET – UNR – AMU), 27 de Febrero 210 bis (S2000EZA), Rosario, Argentina

^b Universidad Nacional de Rosario, FCEIA, EIE – Dpto. Control, Pellegrini 250 (S2000EZA), Rosario, Argentina

^c Universidad Tecnologica Nacional – FRRo, Zeballos 1341 (S2000BQA), Rosario, Argentina

ARTICLE INFO

Article history:

Received 24 April 2012

Received in revised form 11 January 2013

Accepted 21 January 2013

Available online xxx

Keywords:

Plantwide control

Decentralized control

Systematic methodology

Pulp mill process

Large-scale process

ABSTRACT

The plantwide control (PWC) complexity increases for highly-integrated and large-scale chemical processes. This work presents a novel framework for decentralized PWC which includes: (i) the selection of the controlled variables (CVs), (ii) the pairing between the manipulated variables (MVs) and the CVs, and (iii) the determination of the controller algorithms as well as their tuning parameters for closed-loop operation. The proposal is to solve the steps (i) and (ii) simultaneously, driving the selection of the most effective PWC structure from a Pareto optimal set. Here, algorithms based only on steady-state information are considered to give a systematic procedure which tries to minimize the use of heuristic considerations. Genetic algorithms (GA) and the Hungarian algorithm (HA) are used here because they provide a good trade-off between computational effort and acceptable results. The proposed methodology is completely tested in a pulp mill benchmark and compared with a previous one.

© 2013 Elsevier Ltd. All rights reserved.

1. Introduction

Typical chemical processes consist of many interconnected unit operations, recycle streams and energy integration, resulting in highly coupled dynamics. In order to satisfy safe process operations, environmental regulations, product quality and maximize profits in this kind of processes, an efficient control structure design from plantwide perspective is necessary (Buckley, 1964). In this challenging scenario, the control problem complexity increases heavily for big processes because a great number of variables are involved.

Over the last decades, the process control community has developed a broad spectrum of PWC methodologies for addressing the design problem in a complete plant. Depending on the approach used to develop the PWC strategy, the methodologies can be based on heuristics (Konda, Rangaiah, & Krishnaswamy, 2005; Luyben, Tyreus, & Luyben, 1998; Vasudevan, Rangaiah, Konda, & Tay, 2009), mathematics (Cao & Kariwala, 2008), optimization (Ochoa,

Wozny, & Repke, 2010; Sharifzadeh & Thornhill, 2012), or mixed approaches (Basualdo, Feroldi, & Outbib, 2012; Chen, McAvoy, & Zafiriou, 2004; Molina, Zumoffen, & Basualdo, 2011; Skogestad, 2000, 2004). An excellent review of PWC methodologies was presented by Vasudevan et al. (2009). Beyond the above classification, it is important that the approach can consider the many topics that arise in the PWC structure design (Downs & Skogestad, 2011). In particular, methodologies with a good degree of systematics are attractive especially when large-scale case studies are analyzed. However, most previous works have mainly considered the Tennessee Eastman (TE) problem (Downs & Vogel, 1993), the toluene hydrodealkylation (HDA) plant (Stephanopoulos, 1984) and the vinyl acetate monomer (VAM) plant (Luyben et al., 1998). In this context, there is still a need to face larger highly integrated processes so as to comprehend the complex nature of the problem, and the many issues that need to be solved.

According to this, the complete benchmark of a pulp mill process introduced by Castro and Doyle (2004b) is studied in the present work in order to design and test a PWC structure. This complex case study introduces several features of interest including: lead/lag responses, large time delays and nonlinearities, inverse responses and slow settling times. The dimension of the process (114 CVs, 82 MVs, and 58 disturbances) and the presence of strong interactions represent a great challenge in terms of PWC. Only Castro and Doyle (2004a) has considered this benchmark for PWC studies.

* Corresponding author at: Computer Aided Process Engineering Group (CAPEG), French Argentine International Center for Information and Systems Sciences (CIFASIS – CONICET – UNR – AMU), 27 de Febrero 210 bis (S2000EZA), Rosario, Argentina. Tel.: +54 3414237248.

E-mail addresses: luppi@cifasis-conicet.gov.ar (P.A. Luppi), zumoffen@cifasis-conicet.gov.ar (D.A.R. Zumoffen), basualdo@cifasis-conicet.gov.ar (M.S. Basualdo).

In this work, the selection of the CVs is based on the sum of square deviations (SSD index) of the uncontrolled variables (UVs) from their operating points, assuming that the other measurements are under perfect control at steady-state. This searching procedure can be found in Molina et al. (2011) and it is implemented here via genetic algorithm (GA). Generally, the CVs selection problem is related to monitoring, identification or fault detection. The advantage of the proposed SSD-based methodology is that it allows to include the control objectives easily through some weighting matrices. On the other hand, the control configuration (i.e. input–output pairings) is based on the overall pairing measure (OPM index) (Fatehi & Shariati, 2007) which accounts the degree of interaction among the control structure. The pairing task is still an open problem and an excellent review of strategies are given in Khaki-Sedigh and Moaveni (2009). Here, a novel procedure which integrates the CVs selection with the CVs–MVs pairing is presented. This methodology proposes to select the final control structure from a Pareto optimal set by trading-off the SSD and OPM indexes. In other approaches (Molina et al., 2011; Sharifzadeh & Thornhill, 2012) these steps are applied sequentially. As each step has an effect on the other, a sequential procedure might generate suboptimal solutions. Moreover, it is common to utilize process-based experience and engineering judgment in order to pair the CVs with MVs for small-medium processes (Luyben et al., 1998; Sharifzadeh & Thornhill, 2012). However, for large-scale systems this procedure might become not practical because the number of alternative designs increases dramatically. In this context, the proposed methodology considers tools as the normalized relative gain array (NRGA) and the Hungarian Algorithm (HA) in order to give a systematic procedure, minimizing heuristic considerations. A comparison with a branch and bound solution (Kariwala & Cao, 2010) is proposed to test the computational efficiency of the HA in large-scale systems.

The proposed architecture is decentralized and can be implemented with P/PI controllers. Downs and Skogestad (2011) argues that methodologies for PWC design are needed such that do not use complex control technology and that do not require the control experts participation. This concept is clearly applied in the industry, where the decentralized approach is still predominant, being the simplest of the PWC structures.

In Castro and Doyle (2004a) a heuristic was utilized to develop a PWC decentralized strategy for the entire pulp mill process. It incorporates many regulatory control loops, as well as cascade control and Kappa factor control. Here, the control strategies are compared through closed-loop simulations of the rigorous nonlinear process model including several disturbances and setpoint changes. The evaluation is based on their capacity to reduce the total error by quantifying the error improvement percent (EIP). Also, the profit improvement percent (PIP) index is used in order to analyze the operating profits.

The contributions of this paper are: (i) a novel plantwide decentralized methodology for large-scale processes, based on both the sum of square deviations and the overall pairing measure concepts, (ii) the new approach integrates algorithms computationally efficient to give a systematic tool which minimizes the heuristic load, (iii) a proposal based on Internal Model Control (IMC) which provides controller tuning for the very large number of PI control implementations, (iv) to perform a dynamic evaluation on a big case study, (v) to compare the developed PWC strategy with other approach.

The paper is organized as follows: the next section presents the systematic PWC design methodology, detailing its background and tools. Section 3 starts with a brief description of the pulp mill process and its objectives, and continues with the application of the developed PWC design methodology to the case study. Section 4 presents the simulation results, including an analysis of the

Table 1
PWC design methodology.

Step	Description
A. Preliminary tasks	Define the stabilizing control loops (Section 2.1)
1. Process stabilization:	Obtain a reduced process model (Section 2.1)
2. Model identification:	
B. Steady-state design stage	Select the CVs set together with the optimal CVs–MVs pairing (Section 2.2)
3. Control configuration:	
C. Dynamic evaluation stage	Determine the algorithm and tuning parameters for each control loop (Section 2.3)
4. Controllers tuning:	Evaluate the dynamic performance of the designed strategy (Section 2.4)
5. Closed-loop analysis:	

dynamic behavior and the operation costs of the obtained control structure. Finally, in Section 5 the conclusions and future works are exposed.

2. Plantwide control design methodology

In this section, the PWC design procedure is presented. The main tasks of the methodology are schematically given in Table 1, represented by five sequential steps. The control configuration step constitutes the principal contribution and it is summarized in Section 2.2.3.

2.1. Process stabilization and model identification

The pulp mill process is open-loop unstable, therefore it is necessary to stabilize the plant through a certain number of control loops. Generally, these control loops are related to level or pressure in tanks and vessels, given its pure integrative behavior. The methods presented by Arkun and Downs (1990) and McAvoy (1998) are helpful to achieve the process stabilization with a minimum number of control loops.

Once all the unstable modes of the process are stabilized, different system identification techniques can be applied in order to obtain reduced order models. Steady-state gains and also simplified dynamic linear models can be estimated as proposed in Section 3.5 for supporting the control configuration and the controller tuning steps, respectively.

2.2. Control configuration

The PWC design methodology proposed here involves the selection of n CVs from a set of m available measurements (being $m > n$), simultaneously with the $n \times n$ CVs–MVs pairing. This procedure only requires steady-state information of the process. A detailed discussion about this issue is presented in the following sections.

2.2.1. Evaluation of CVs sets

The methodology starts with the selection of different CVs sets, based on the minimization of the sum of square deviations (SSD). The SSD approach assumes perfect control in the least square sense, considering that n variables are perfectly controlled at their desired setpoint. The chosen variables guarantee that the $(m - n)$ UVs will remain as close as possible to its nominal operating point even though the disturbances effects and setpoint changes (Basualdo et al., 2012). Therefore, the steady-state SSD index is useful to evaluate and compare different CVs combinations.

Taking into account the well-known IMC structure presented in Fig. 1, at steady state ($s=0$) the UVs can be stated as:

$$\mathbf{y}_r = \mathbf{S}_{sp} \mathbf{y}_s^{set} + \mathbf{S}_d \mathbf{d} \quad (1)$$

where:

$$\mathbf{S}_{sp} = [\mathbf{G}_r \mathbf{G}_s^{-1}] \quad \text{and} \quad \mathbf{S}_d = [\mathbf{D}_r - \mathbf{G}_r \mathbf{G}_s^{-1} \mathbf{D}_s] \quad (2)$$

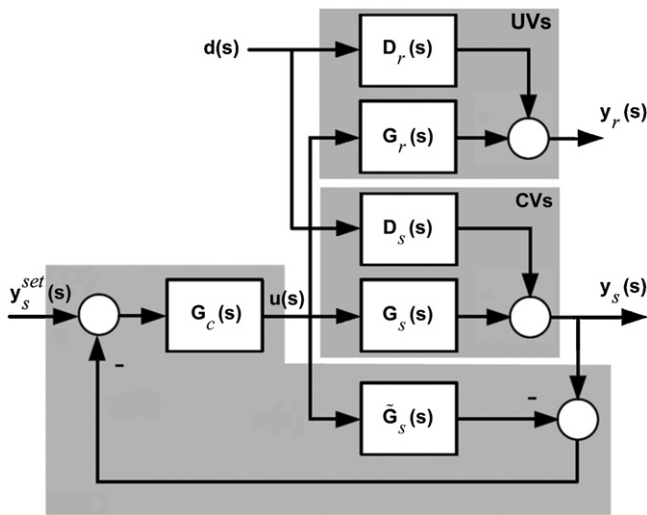


Fig. 1. IMC structure.

Here, $\mathbf{G}_s(s)$, $\mathbf{D}_s(s)$, $\mathbf{G}_r(s)$ and $\mathbf{D}_r(s)$ are transfer function matrices of $n \times n$, $n \times p$, $(m-n) \times n$, and $(m-n) \times p$, respectively. The vectors \mathbf{y}_s^{set} and $\mathbf{d}(s)$ of dimension $n \times 1$ and $p \times 1$ are setpoint and disturbance vectors, respectively. As can be seen from Eqs. (1) and (2), the deviation of the UVs respect to its nominal operating point depends specifically on the CVs selection through \mathbf{G}_s . Therefore, the idea is to choose those CVs to minimize the following criteria:

$$SSD = \text{tr}[\Lambda_1^2 \mathbf{S}_{sp}^T \Lambda_2^2 \mathbf{S}_{sp}] + \text{tr}[\Theta_1^2 \mathbf{S}_d^T \Theta_2^2 \mathbf{S}_d] \quad (3)$$

where Λ_1 and Λ_2 are diagonal matrices that allow to incorporate relative weights according to the magnitude of the setpoints, and the importance between the considered outputs, respectively. Θ_1 and Θ_2 play the same role as Λ_1 and Λ_2 for the disturbances, and $\text{tr}[\cdot]$ represents the trace of the matrix. By this way, the main control objectives of the process can be effectively incorporated. Appendix C in Molina et al. (2011) shows that the minimization of Eq. (3) drives to select the best rows of $\mathbf{G}(s)$ to construct $\mathbf{G}_s(s)$ such that the matrix conditioning of $\mathbf{G}_s(s)$ tends to be improved by increasing its minimum singular value. This implies good controllability of $\mathbf{G}_s(s)$ and therefore the required control energy (deviations in the manipulated variables) will not be excessive. It is known that ill-conditioned processes are essentially difficult to control (Skogestad & Postlethwaite, 2005).

Considering m available measures and n potential CVs, the problem is to select a set of n variables from m such that the criterion in Eq. (3) is minimized. This problem requires to do a great number of combinations $m!/[n!(m-n)!]$ in order to find the optimal solution. For this reason, an exhaustive search is unpractical for large-scale processes. Genetic algorithm (GA) is a stochastic global optimization method which proposes a generalized treatment for these problems, with the advantage that it produces a set with the best solutions (sorted from the optimal one to the following suboptimal solutions). This is an important result to evaluate several possible control structures. Even though the GA is able to solve problems of very large dimension, it does not guarantee a global minimum. However, a great number of applications using GA exists with acceptable results (Molina et al., 2011; Sharifzadeh & Thornhill, 2012).

Using GA, the combinatorial problem can be stated as in Eq. (4):

$$\begin{aligned} \min_{\mathbf{C}_i} SSD(\mathbf{C}_i) = \min_{\mathbf{C}_i} & \left[\text{tr}[\Lambda_1^2 \mathbf{S}_{sp}^T(\mathbf{C}_i) \Lambda_2^2 \mathbf{S}_{sp}(\mathbf{C}_i)] \right. \\ & \left. + \text{tr}[\Theta_1^2 \mathbf{S}_d^T(\mathbf{C}_i) \Theta_2^2 \mathbf{S}_d(\mathbf{C}_i)] \right] \end{aligned} \quad (4)$$

subject to:

$$\det(\mathbf{G}_s(\mathbf{C}_i)) \neq 0 \quad (5)$$

$\mathbf{C}_i = [c_1, \dots, c_m]$ represents a binary chromosome. Here, $c_j = 1$ indicates that the measure corresponding to the location j is controlled, and $c_j = 0$ the opposite situation. The constraint in Eq. (5) guarantees that the optimal solution for Eq. (4) is feasible.

The SSD index evolution over the last GA generations (solutions) presents a typical flat zone, where its magnitude results very close to the minimum (last solution). Taking into account a set of solutions inside this zone it is possible to obtain the optimal CVs–MVs pairing corresponding to each solution, where *optimal* refers to the CVs–MVs pairing which presents the smallest interaction effect. In the following, Section 2.2.2 presents a scalar index able to quantify this interaction effect.

2.2.2. Optimal CVs–MVs pairing

The well-known relative gain array (RGA) presented by Bristol (1966) has been a powerful tool for supporting the pairing selection problem in small-medium scale square processes. A review of the pairing criterion using RGA and proposed modifications can be found in Khaki-Sedigh and Moaveni (2009).

In the context of CVs–MVs pairing by RGA, the selection among pairs with RGA values in either side of 1 might be confusing. Interaction and robustness result different for the case of two pairs which have RGA values at the same distance from 1. However, it is possible to normalize this behavior by mapping each element λ_{ij} of the RGA through a nonlinear function f which drives to the NRGA (Fatehi & Shariati, 2007). This allows to select rigorously and systematically the best pairing among existing options. Thus, if φ_{ij} represents each element of the NRGA, the pairing criterion recommends: (i) avoid pairings with zero values of φ_{ij} , (ii) select pairs with large φ_{ij} , (iii) the selected pairs should satisfy the Niederlinski condition (Appendix A). The optimal pairing selection can be obtained from the solution of the next conditional assignment problem:

$$\Psi = \max \sum_{P_s} \varphi_{ij} \quad (6)$$

where P_s represents the overall pairing which satisfies the NRGA criterions given above. And Ψ is a scalar index called *overall pairing measure* (OPM). The HA proposed by Cooper and Steinberg (1974) is a systematic method that solves efficiently assignment problems. It produces acceptable results with minimal computational effort.

The OPM index represents a measure of the interaction effect among the control loops, so it is useful for comparison purposes. A lower value of OPM corresponds to a structure which has a higher interaction effect. This behavior is not desirable for implementing a decentralized control structure. In the following Section 2.2.3 the novel decentralized PWC methodology is presented. The control structures corresponding to the set of solutions with similar SSD index are compared according to their OPM.

2.2.3. Overall procedure

The proposed procedure can be summarized as follows:

- 1 Execute the procedure based on GA described in Section 2.2.1 to find the minimum SSD index.
- 2 From step 1, select the set of solutions which SSD value is in the small range of variation around the minimum (last solution).
- 3 For each solution selected in step 2:
 - a. Construct the square matrix \mathbf{G}_s according to the current set of selected CVs.
 - b. Obtain the corresponding RGA. Some RGA values could be filtered in order to avoid unwanted CVs–MVs pairings (for instance, pairings associated with RGA values smaller than 0.5).

- c. From the (filtered) RGA, obtain the associated NRGA given by $\varphi_{ij} = f(\lambda_{ij})$.
- d. From the NRGA, use the HA in order to obtain the optimal CVs–MVs pairing, and the corresponding OPM index value.
- e. Evaluate the associated Niederlinski index (*NI*) given by Eq. (22) (Appendix A)

4 From step 3, consider only the subset of solutions with *NI*>0.
 5 The final solution must be selected from the Pareto optimal set by trading-off the SSD and OPM indexes.

The proposed methodology only considers optimal sets (in the OPM sense) with *NI*>0 (step 4). However, if all the solutions from step 3 present *NI*<0, then the Appendix B in Fatehi and Shariati (2007) explains how to obtain suboptimal pairings. This might requires several search-check-search loops to find solutions with *NI*>0.

The selected decentralized structure can be implemented with P/PI controllers. In the following section, the controller design is described in detail through the Internal Model Control (IMC) theory which is based on the linear models commented in Section 2.1.

2.3. Controllers tuning

The tuning procedure allows to evaluate the closed-loop dynamic response of the PWC structure in order to demonstrate the potentiality of the methodology. The idea is to check that all control objectives are satisfied and the control energy expenditure is suitable.

Following the IMC theory, the transfer function matrix of the model can be factorized by an invertible and a non-invertible part, and the controller is given by:

$$\mathbf{G}_c(s) = \tilde{\mathbf{G}}_s^-(s)^{-1} \mathbf{F}(s) \quad (7)$$

where $\tilde{\mathbf{G}}_s^-(s)$ is the invertible part of the model, and $\mathbf{F}(s) = \text{diag}([1/(\tau_{f1}s+1)^{\kappa_1} \dots 1/(\tau_{fn}s+1)^{\kappa_n}])$ is the transfer function matrix of the low-pass filter such that $\mathbf{G}_c(s)$ be proper. If the process model does not present any non-invertible part, then the IMC approach can be converted to an unitary feedback control policy by:

$$\mathbf{G}_c^*(s) = \tilde{\mathbf{G}}_s^-(s)^{-1} \mathbf{F}(s) [\mathbf{I} - \mathbf{F}(s)]^{-1} \quad (8)$$

The robustness criteria presented in Rivera (1986, 2007) for the single-input single-output (SISO) case can be used in order to tune this generalized control structure. When there is no delay in the control loop, the criterion is $0 < \tau_{fi} < \tau_i^m$ in order to improve the closed loop time response. Here, τ_{fi} represents the filter time constant which affect the input channel i , and τ_i^m is the time constant of the process model for the loop i . On the other hand, if time delay θ_i exists, it is suggested that $\tau_{fi} > \theta_i$. Finally, the tuning parameters for each control loop can be obtained through:

$$\mathbf{K}_c = \frac{\tau_i^m + \theta_i/2}{K_m(\tau_{fi} + \theta_i/2)} \quad (9)$$

$$\mathbf{T}_i = \tau_i^m + \frac{\theta_i}{2} \quad (10)$$

where K_m is the static gain, τ_i^m is the time constant, and θ_i is the time delay of the process model. This approach generally produces good results for decentralized MIMO control structures.

2.4. Closed-loop analysis

This analysis is based on the dynamics of the CVs and the MVs when the controlled process is subject to pre-determined disturbances and setpoint changes. For this purpose, two indexes are considered: the error improvement percent (EIP), and the profit

improvement percent (PIP). These are defined as follows, taking into account the integral absolute error (IAE) and the total operating profit (TOP) definitions:

1 Integral absolute error (IAE):

$$\text{IAE} = \sum_k |r(k) - y(k)| \quad (11)$$

The IAE index can be computed for each controlled variable y , where r represents the corresponding setpoint.

2 Error improvement percent (EIP):

$$\text{EIP} = \frac{\text{IAE}^{\text{base}} - \text{IAE}^{\text{new}}}{\text{IAE}^{\text{base}}} \cdot 100 \quad (12)$$

where *base* refers to a decentralized control strategy proposed as reference, and *new* denotes the PWC design developed in this work. The EIP index can be obtained for each CV. The *new* control strategy is better than the *base* one if the EIP index is positive.

3 Total operating profit (TOP):

$$\text{TOP} = \text{Sales} - \text{Penalty Costs} - \text{Raw Costs} \quad (13)$$

The TOP involves the sum of raw material costs, penalty costs, and the profits made from sales of products.

4 Profit improvement percent (PIP):

$$\text{PIP} = \frac{\text{TOP}^{\text{new}} - \text{TOP}^{\text{base}}}{|\text{TOP}^{\text{base}}|} \cdot 100 \quad (14)$$

Finally, the PIP index considers the increased profits between the *base* control strategy and the *new* control strategy. From an economical point of view, a positive PIP means that the new control strategy increases the operating profits.

The scores in the EIP and PIP allows to compare different control strategies according to their performance.

3. Plantwide control of the pulp mill process

In this section, the complete methodology for PWC design described in Section 2 is applied to the large-scale pulp mill process presented by Castro and Doyle (2004b).

3.1. Case study: pulp mill process

3.1.1. Process description

A simplified flow sheet of the pulp mill process is shown in Fig. 2 obtained from the work of Castro and Doyle (2004b). The process consists of two major areas such as the fiber line and the recovery plant.

The objective of the fiber line is to produce fibers from wood chips at a desired production rate and quality. Major raw materials of this process are wood chips and chemicals called white liquor (WL) which consists primarily of NaOH and NaSH.

The most important objectives of the chemical recovery area are to obtain energy from the combustion of black liquor and to regenerate the NaOH and Na₂S from the weak black liquor coming from the digester, extract liquor flows and the brown stock washing system. A complete description of the pulp mill process can be found in Castro and Doyle (2004b).

3.1.2. Process objectives

The objectives of the process (product quality, production rate, etc.) and the process constraints (operational, safety and environmental) are specified in Tables 1, 3 and 4 in Castro and Doyle (2004b). The main goal is to produce pulp with a desired brightness and production rate, with minimum cost.

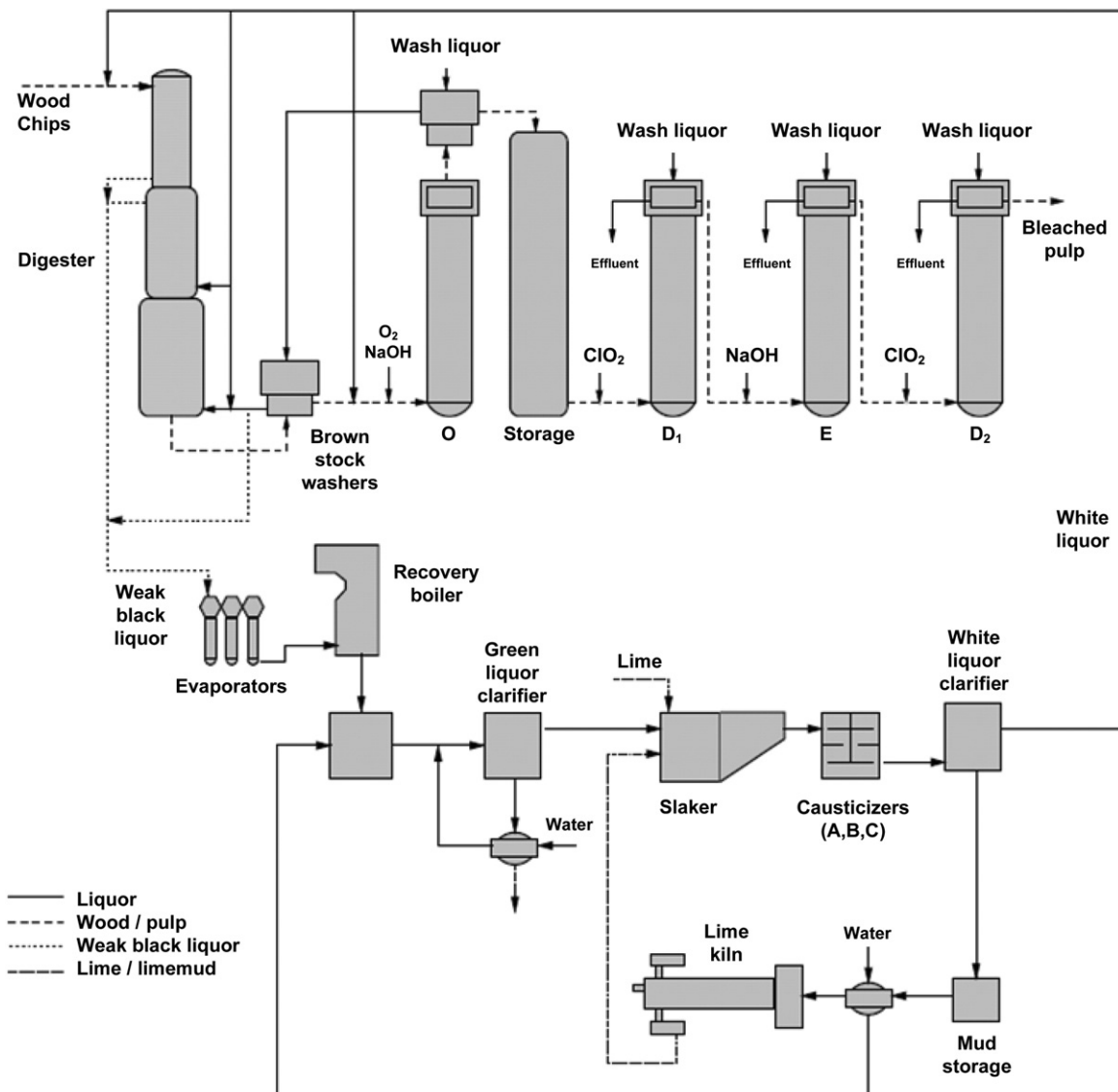


Fig. 2. The pulp mill process. Schematic diagram.

In the present work it is assumed that the process operates under nominal conditions, with a production rate of 630 tons/day, E Kappa number of 2.50 and D_2 Brightness equal to 0.81. This corresponds to the default configuration of the benchmark problem.

The detail of the mathematical models as well as the computational code corresponding to the unit operations are available as a benchmark problem for download from the Doyle's Group web site (Doyle, 2002).

3.2. Initial considerations

In this case study, a total of 114 CVs and 82 MVs are initially available in order to control the process. The nomenclature used for all the CVs, MVs, and DVs is the same as that given in Castro and Doyle (2004b). The complete list of process variables is available in Tables 13–18 in Appendix F.

3.3. Process stabilization

It was determined that the levels in the storage tank (CV34), D₂ tower (CV38), smelt dissolving tank (CV53), storage tank no. 1

(CV57), mud mixing tank (CV73) and storage tank no. 2 (CV74), and the smelt dissolving tank condensate temperature (CV55) should be controlled in order to stabilize the process.

The corresponding CVs–MVs pairing, as well as its tuning parameters were adopted to be the same as in Castro and Doyle (2004b). These stabilizing control loops are indicated in Table 2.

The correct operation of this stabilizing configuration was tested through step-test simulations of the rigorous nonlinear process model. If any of these loops is disconnected, then the system becomes unstable for small step inputs.

Table 2
Stabilizing control loops.

CV no.	MV no.	K_c	T_i
34	18	-1.67	–
38	38	-5.0	–
53	62	5.0	–
55	81	-0.005	30
57	46	3.0	–
73	60	-2.92	–
74	63	-2.92	–

3.4. Available variables for identification

Once the process is stabilized through the control loops shown in Table 2, the available number of variables to be considered for model identification has been reduced from 82 MVs and 114 CVs, to 75 MVs and 107 CVs. Concerning the disturbances, only those that were effectively accounted by Castro and Doyle (2004b) are considered here for the model identification. This includes a total of 13 DVs: wood densities no. 1, 2, 3, 4, 5, 6 and 7 (DV2 to DV8), D_1 ClO₂ stream composition (DV14), D_2 ClO₂ stream composition (DV19), dregs DR (DV45), ambient temperature (DV48), filter 1 DR (DV54) and filter 2 DR (DV56). Due to the additional considerations detailed in Appendix C, the total number of variables for model identification results 74 MVs, 105 CVs and 13 DVs.

3.5. Model identification

Here, the stabilized rigorous nonlinear model is considered in order to apply system identification techniques. This procedure allows to obtain both the steady-state gains and the dynamic linearized models corresponding to the input–output variables of the process.

The experiments are based on step-tests implemented in the Matlab environment (Ljung, 1999, 2002). Hence, each specific input is excited with a step of +1% above its nominal operating point, and the output data is collected periodically with a suitable sample time ($T_s = 5$ min is adopted, the same as Castro and Doyle (2004b)). This amplitude of excitation results large enough to make the process responses clearly visible. It is not too large to avoid nonlinearities.

The data is normalized using scaling factors (Castro & Doyle, 2004b) before starting the model identification procedure. For a given input mv_i and output cv_k , the corresponding normalized steady-state gain $g_{k,i}$ is obtained as:

$$g_{k,i} = \frac{cv_{k_{final}} - cv_{k_{ss}}}{mv_{i_{final}} - mv_{i_{ss}}} \frac{\Delta mv_{i_{max}}}{\Delta cv_{k_{max}}} \quad (15)$$

where $cv_{k_{final}}$ and $mv_{i_{final}}$ are the unscaled final values, $cv_{k_{ss}}$ and $mv_{i_{ss}}$ are the steady-state values, and $\Delta cv_{k_{max}}$ and $\Delta mv_{i_{max}}$ represent the maximum range of variation of the input mv_i and output cv_k , respectively. The obtained $g_{k,i}$ conforms the normalized steady-state gain matrix G , which has dimension 105×74 . The same procedure is performed taking into account the disturbances, obtaining the normalized steady-state gain matrix D of dimension 105×13 .

On the other hand, first order with and without time delay transfer functions are identified using the *pem* algorithm Ljung (2002) obtaining linear, low-order, continuous-time transfer function models with the following structure:

$$H(s) = \frac{K_p}{1 + T_{p1}s} e^{-T_{ds}} \quad (16)$$

where K_p is the static gain, T_{p1} is the time constant, and T_{ds} is the time delay. The cited algorithm allows to estimate the model parameters from the data, by using an iterative prediction-error minimization method. The obtained dynamic linear models are suitable for the controllers design, using the IMC tuning method presented by Rivera (2007).

3.6. Control configuration

The design procedure continues with the generation of several CVs sets as described in Section 2.2.1. For a particular set, the methodology requires to compute G_s^{-1} (Eq. (2)). For this purpose, the GA discards as possible solutions those CVs sets such that $\det(G_s) = 0$ (unfeasible solution). In Appendix D an analysis of the

G matrix is additionally presented. The objective is to determine which columns/rows of G should be removed before the execution of the GA in order to avoid unfeasible solutions. After the matrix analysis, the number of variables to be considered for the control configuration step has been reduced from 74 MVs and 105 CVs, to 57 MVs and 93 CVs.

On the other hand, due to pulp mill process requirements (Section 3.1.2) the D_2 production rate (CV3), the E kappa number (CV22) and the D_2 brightness (CV26) must be controlled. Additionally, the E tower temperature (CV23), the D_2 tower temperature (CV25), the kiln O₂ mass fraction (CV79) and the kiln CaCO₃ mass fraction (CV81) have to be controlled because their corresponding setpoints are selected to be modified during the closed-loop tests (Section 4). A total of 7 CVs must be controlled.

In this context, the problem is to select $57 - 7 = 50$ CVs from a total of $93 - 7 = 86$ available measurements. This is a combinatorial problem where the number of combinations results $86!/(50!(86-50)!) = 2.14 \times 10^{24}$.

The problem to solve is:

$$\min_{\mathbf{C}_i^*} \text{SSD}(\mathbf{C}_i^*) = \min_{\mathbf{C}_i^*} [tr[\Lambda_1^2 \mathbf{S}_{sp}^T(\mathbf{C}_i^*) \Lambda_2^2 \mathbf{S}_{sp}(\mathbf{C}_i^*)] \\ + tr[\Theta_1^2 \mathbf{S}_d^T(\mathbf{C}_i^*) \Theta_2^2 \mathbf{S}_d(\mathbf{C}_i^*)]] \quad (17)$$

subject to:

$$\mathbf{C}_i^*(j) = [C_i(1 : 2), 1, C_i(3 : 17), 1, 1, C_i(18), 1, 1, \\ C_i(19 : 59), 1, 1, C_i(60 : 86)] \quad (18)$$

$$\sum_{j=1}^{86} C_i(j) = 50 \quad (19)$$

$$\det(\mathbf{G}_s(\mathbf{C}_i^*)) \neq 0 \quad (20)$$

where C_i represents the search chromosome. The fixed 1's in \mathbf{C}_i^* indicate that the corresponding measures are controlled (CV3, CV22, CV26, CV23, CV25, CV79 and CV81). Λ_1 is defined as a diagonal matrix of dimension 57×57 , which has a weight value of 1 in the positions corresponding to these CVs, and 0.1 in the rest. In addition, the configuration $\Lambda_2 = I_{36}$ and $\Theta_2 = I_{36}$ implies equal relative weight between variables, where I_i represents the identity matrix of dimension $i \times i$. By setting $\Theta_1 = I_{13}$, all perturbations are considered with the same weight.

The GA was executed with the settings shown in Table 3 and the weight matrices defined above. Its execution was repeated several times (using the same configuration) but starting from different initial populations (chosen randomly). In all cases it was verified that the optimal solution was the same. In addition, all GA executions ran long time in order to achieve the stabilization of the SSD index. Otherwise, the obtained solutions would have SSD indexes far from the optimum (undesirable).

As shown in Fig. 3a, the GA evolves towards the optimal solution reducing the value of the SSD index along its generations. Fig. 3b shows the evolution of the percentage of unfeasible solutions during this search process. The SSD index has very similar values from solution $L = 183$ to the last generation, presenting a typical flat zone.

Therefore, the set of solutions from generation $L = 183$ to $L = 500$ were considered for the step 3 of the procedure (Section 2.2.3). For each solution, the corresponding RGA was filtered in order to avoid pairings with RGA values smaller than 0.3. Finally, the NRGA, the optimal CVs–MVs pairing, the associated OPM index, and the NI

Table 3
Genetic algorithm parameters.

N_i (Initial population)	N_c (No. of potential CVs)	n (No. of CVs to be selected)	N_g (No. of generations)	Mutation Probability	Crossover Probability	Selection
13,000	86	50	500	$0.7/N_c$	0.7	Roulette wheel

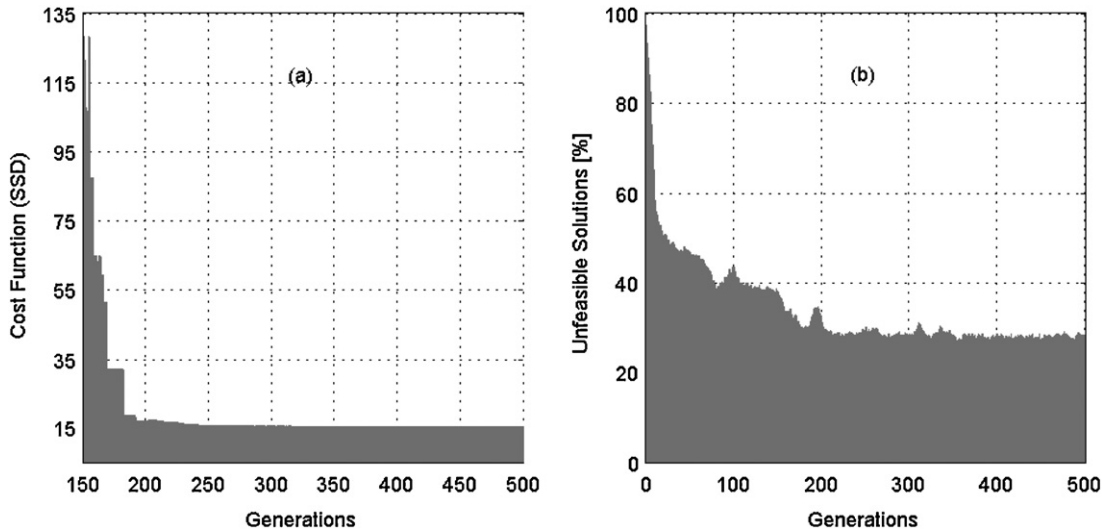


Fig. 3. GA evolution: SSD index and percentage of unfeasible solutions.

were calculated for each solution. The following typical normalization function $f(\lambda)$ was used for NRGA calculations:

$$f(\lambda) = \begin{cases} 0, & \lambda \leq 0 \\ \lambda, & 0 < \lambda \leq 1 \\ e^{(1-\lambda)/4}, & 1 < \lambda \end{cases} \quad (21)$$

Fig. 4 shows all feasible solutions corresponding to the flat zone with $NI > 0$, where only points B and M belong to the Pareto optimal set. In Table 4 the corresponding values are presented. Smaller values of SSD (x -axis) and $(OPM_0 - OPM)$ (y -axis) are preferred to larger ones. Here, $OPM_0 = 57$ represents the best OPM that a decentralized control structure of dimension 57×57 can achieve.

Solution $L = 193$ (point B) presents a SSD index degradation of 11.2% respect to solution $L = 349$ (point M), but presents the maximum OPM value. On the other hand, solution $L = 349$ (point M) degrades 1.1% the OPM respect to solution $L = 193$ (point B), but presents the minimum SSD value. Therefore, solution $L = 349$ (point M) is finally selected due to its good trade-off between SSD and OPM values:

This solution suggests to select the CVs no. 3, 5, 7, 12, 14, 15, 17, 18, 19, 20, 21, 22, 23, 24, 25, 26, 28, 29, 30, 31, 32, 33, 35, 36, 37, 40, 41, 43, 44, 49, 50, 52, 56, 59, 60, 61, 62, 63, 72, 75, 76, 77, 78, 79, 81, 82, 86, 91, 92, 93, 96, 98, 99, 106, 112, 113, and 114.

The final CVs–MVs interconnection is obtained in a systematically way through the NRGA-HA algorithm, as described in the step 3 of Section 2.2.3. The performance of this procedure was compared against a branch and bound solution proposed by Kariwala and Cao (2010), as shown in Appendix B.

In Fig. 5 the NRGA matrix of the system is presented. The MVs (x -axis) have been rearranged in order to group the selected elements in the diagonal. A close examination of the NRGA shows that there are sub-blocks where the interactions of the process are important. This seriously difficult the implementation of the controllers. Tables 11 and 12 in Appendix E show the complete input–output pairing as well as the controllers parameters obtained according to the IMC procedure (Section 2.3).

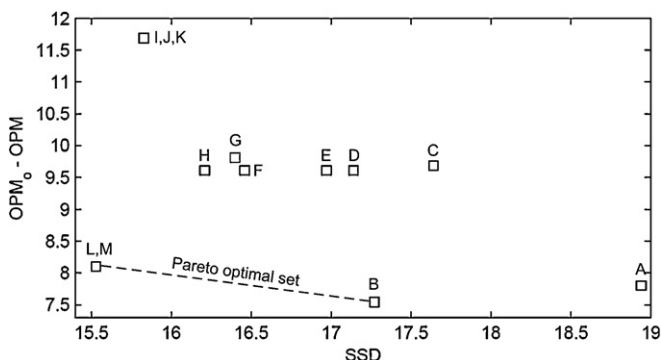


Fig. 4. Feasible solutions corresponding to the flat zone with $NI > 0$.

Table 4
SSD and OPM values corresponding to the solutions of the flat zone with $NI > 0$.

Point	L (generation no.)	SSD index	OPM index	$\text{OPM}_0 - \text{OPM}$
A	183–188	18.94	49.20	7.80
B	193–202	17.27	49.46	7.54
C	203–208	17.64	47.32	9.68
D	209–214	17.14	47.39	9.61
E	215–225	16.97	47.39	9.61
F	226–230	16.46	47.39	9.61
G	231–239	16.40	47.19	9.81
H	240–241	16.21	47.39	9.61
I	261	15.83	45.31	11.69
J	263–275	15.83	45.31	11.69
K	277–283	15.83	45.31	11.69
L	311	15.53	48.90	8.10
M	316–349	15.53	48.90	8.10

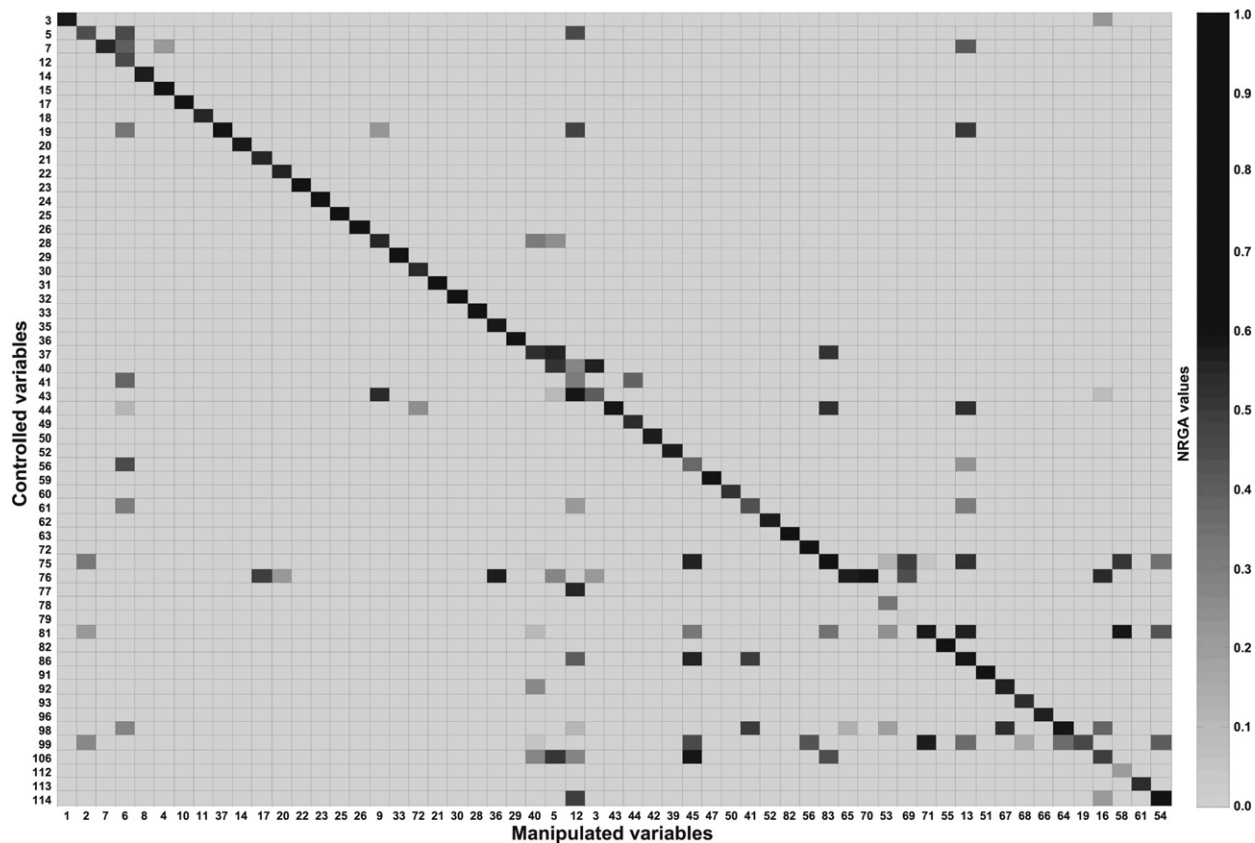


Fig. 5. NRGA matrix of the process.

4. Closed-loop analysis

Closed-loop simulations of the complete nonlinear model were done to evaluate the performance of the developed PWC structure. The applied disturbance/setpoint sequence is described in [Table 5](#).

[Figs. 6–10](#) show the closed-loop responses corresponding to key variables of the process, where the *new* strategy is confronted with that proposed by [Castro and Doyle \(2004a\)](#) (*base*).

Table 5
Setpoint/disturbance sequence applied to the process.

Time [h]	Event	Associated var.	Value (scaled)
0	Kiln O ₂ % change	CV79	-1.0
0	Kiln CaCO ₃ % change	CV81	-1.0
8.3	Wood chips density no.1 change	DV40	0.2327
8.3	Wood chips density no.2 change	DV41	0.0872
8.3	Wood chips density no.3 change	DV42	0.2908
8.3	Wood chips density no.4 change	DV43	0.1551
8.3	Wood chips density no.5 change	DV44	0.4265
8.3	Wood chips density no.7 change	DV46	-1.0
25	Wood chips density no.2 change	DV41	0.25
25	Wood chips density no.3 change	DV42	-0.25
41.6	D ₁ ClO ₂ stream composition change	DV52	-0.5
41.6	D ₂ ClO ₂ stream composition change	DV57	-0.5
56.6	Kiln O ₂ % change	CV79	-1.125
75	Ambient temperature change	DV130	-1.0
83.3	Dregs displacement ratio change	DV127	-1.0
83.3	Filter 1 displacement ratio change	DV136	-1.0
83.3	Filter 2 displacement ratio change	DV138	-1.0
91.6	Bleach pulp production change	CV3	0.5
100	E Kappa no. change	CV22	-0.83
100.16	E tower temperature change	CV23	1.5
101.5	D ₂ tower temperature change	CV25	1.5
101.5	D ₂ brightness change	CV26	5.0

Table 6
Dynamic performance comparison.

CV description	IAE (base)	IAE (new)	EIP [%]
D ₂ Production rate (CV3)	126.05	130.84	-3.80
E Tower Kappa no. (CV22)	75.79	266.63	-251.82
E Temperature (CV23)	2.01	2.17	-7.96
D ₂ Temperature (CV25)	2.18	2.60	-18.93
D ₂ Brightness (CV26)	753.63	796.70	-5.72
Black liquor solids % (CV44)	23.76	17.20	27.60
Kiln O ₂ mass fraction (CV79)	401.61	352.23	12.29
Kiln CaCO ₃ (CV81)	221.95	1384	-523.57

[Table 6](#) shows the obtained IAE and EIP indexes presented in [Section 2.4](#). The TOP and PIP indexes corresponding to each operation unit of the process are also included in [Tables 7 and 8](#) in order to analyze the involved control energy expenditure.

[Fig. 6](#) shows the dynamics of the D₂ production rate control loop (CV3-MV1). In [Fig. 6a](#), the tracking of the CV is showed. As can be seen, the new control structure presents good tracking behavior for the setpoint change at t = 91.6 h, with a small increase

Table 7
Economic performance. Original control structure ([Castro & Doyle, 2004a](#)).

Operation unit	Costs [\$]	Penalties [\$]	Sales [\$]	Profits [\$]
Digester	3,218,600	–	11,307,000	8,088,200
Brown stock	8870	–	–	-8870
Oxygen tower	147,170	–	–	-147,170
Bleach plant	1,567,700	256,670	–	-1,824,400
Evaporators	1,700,900	–	1,187,100	-513,870
Recast	360,590	–	–	-360,590
Lime kiln	139,250	2	–	-139,250
Total	7,143,100	256,670	12,494,000	5,094,100

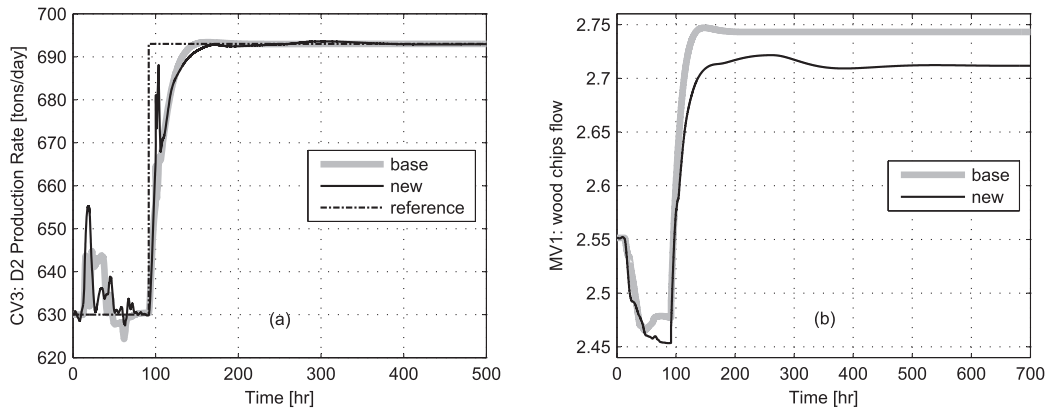


Fig. 6. CV3 and MV1 closed-loop responses.

Table 8
Economic performance comparison.

Operation unit	Costs [\$]	Penalties [\$]	Sales [\$]	Profits [\$]	PIP [%]
Digester	3,173,000	–	11,309,000	8,136,000	0.59
Brown stock	9663	–	–	–9663	–8.94
Oxygen tower	147,400	–	–	–147,400	–0.16
Bleach plant	1,620,300	153,010	–	–1,773,300	2.79
Evaporators	1,663,800	–	1,159,100	–504,760	1.77
Recast	353,160	–	–	–353,160	2.06
Lime Kiln	129,750	–	–	–129,750	6.83
Total	7,097,100	153,010	12,468,000	5,218,000	2.43

in the corresponding IAE value ($EIP = -3.8\%$). The rate of change is similar for both strategies, which produces similar digester sales (see Tables 7 and 8). However, Fig. 6b shows a lower wood chips flow (MV1) which represents a reduced digester operational costs and therefore $PIP = 0.59\%$.

In Fig. 7a, the tracking of the D_2 brightness (CV26) is presented. As can be seen, the new strategy presents acceptable tracking behavior for the setpoint change at $t = 101.5$ h, with a small increase in the corresponding IAE value ($EIP = -5.7\%$). Despite of this, CV26 evolves to the reference faster than the original decentralized strategy and is able to reduce the time during which the quality requirement is not satisfied. This results in an increase of the PIP for this operation unit ($PIP = 2.8\%$).

In Fig. 7b, the tracking of the kiln O_2 mass fraction (CV79) is showed. The new control structure presents good tracking behavior for successive setpoint changes corresponding to $t = 0$ h and $t = 56.6$ h, resulting a reduction of 12.3% in the IAE respect to the original decentralized strategy.

For the E tower temperature (CV23) and the D_2 tower temperature (CV25), the new strategy shows good tracking behavior for setpoint changes corresponding to $t = 100.16$ h and $t = 101.5$ h respectively, with an acceptable increase in the corresponding IAE values: $EIP = -7.9\%$ and $EIP = -18.9\%$, respectively. The associated figures are not depicted here since there are no appreciable differences between the dynamics of both control strategies.

In Fig. 8a, the tracking of the E tower Kappa no. (CV22) is showed. As can be seen, the new PWC is capable of tracking the setpoint change, but presents an increase in the IAE index due to the significant overshoot during setpoint change.

The percentage of black liquor solids (CV44) and the effect 2 steam flow (MV43) are shown in Fig. 9a and b respectively. The new strategy presents good regulatory behavior in presence of disturbances, maintaining the CV44 next to the reference value of 0.65, obtaining a decrease of 27.6% in the IAE index. In addition, MV43 presents a suitable evolution without excessive control energy requirements. In Table 8 it is observed that $PIP = 1.77\%$

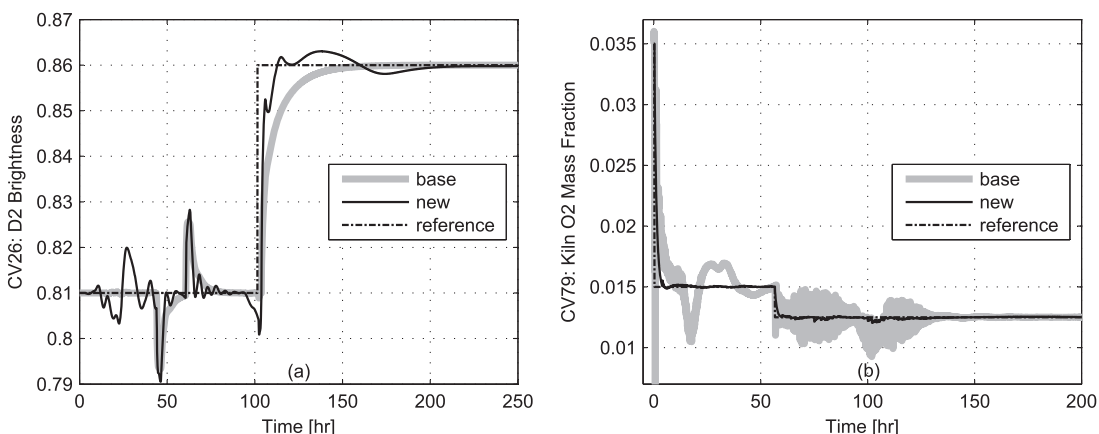


Fig. 7. CV26 and CV79 closed-loop responses.

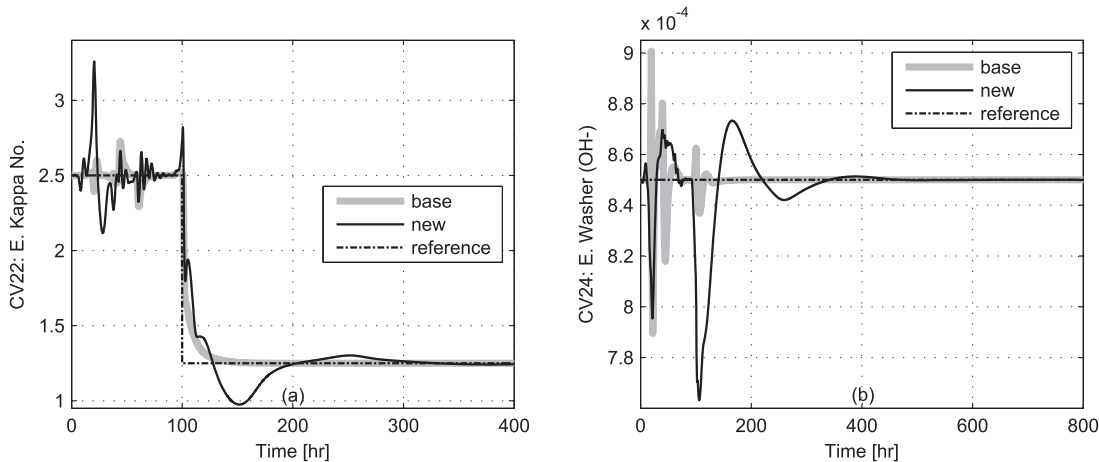


Fig. 8. CV22 and CV24 closed-loop responses.

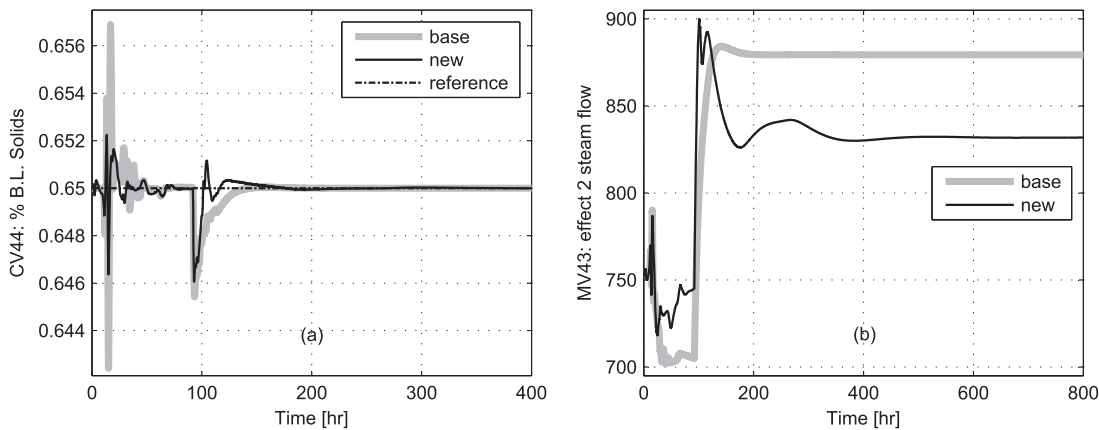


Fig. 9. CV44 and MV43 closed-loop responses.

for the evaporators. This is related to the lower energy of control required by the new control strategy, which in fact reduces the evaporators operational costs.

Fig. 10 shows the dynamics of the kiln CaCO_3 control loop (CV81–MV71). In Fig. 10a, the tracking of the CV is presented. The new structure is capable of tracking the setpoint change at $t=0$ h, but with an increase in IAE value due to the significant overshoot at $t=0$ h. Fig. 10b depicts the kiln fuel flow (MV71), which has a suitable evolution with a smaller consumption of fuel.

For the case of digester Kappa no. (CV5), O Kappa no. (CV19), E washer $[\text{OH}^-]$ (CV24) and slaker temperature (CV62) the new strategy presents poor regulatory performance due to overshoots and slow responses during the transition to the reference value. For instance, Fig. 8b shows the dynamics of the E washer $[\text{OH}^-]$ (CV24).

As shown in Figs. 6b, 9b and 10b, the designed PWC has a steady-state operation point different from the base case. This is due to the fact that the compared control structures have different steady-state multivariable gains.

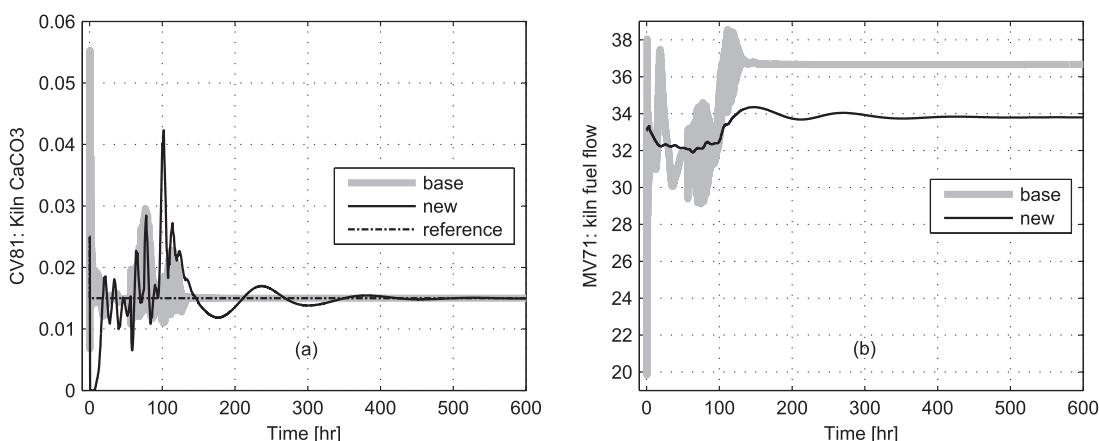


Fig. 10. CV81 and MV71 closed-loop responses.

The proposed decentralized PWC strategy presents acceptable behavior in presence of setpoint changes, but still needs to be improved in order to reject disturbances with better performance. On the other hand, there is a global costs reduction when comparing against the original decentralized strategy proposed by Castro and Doyle (2004a). Thus verifying that the control energy expenditure is suitable.

5. Conclusions and future work

The case study of the pulp mill benchmark problem indicates that the proposed PWC methodology produces workable decentralized control structures for large-scale processes. The approach is based on steady-state information, and tries to reduce the use of heuristic considerations. Only the design of the inventory control system is addressed using engineering insights. In addition, it was shown that minimal computation times are required by the proposed NRGA-HA algorithm in order to solve the large CVs–MVs pairing problem. The achieved results show stable and acceptable dynamic performance under several disturbances and setpoint changes, using only conventional SISO P/PI controllers. This behavior was compared with the strategy proposed by Castro and Doyle (2004a), where additional cascaded PI and Kappa controllers were included.

In a future approach, the problem of MVs selection will be discussed so as to reduce the number of actuators, and therefore the amount of sensors and controllers to be installed, minimizing the investment cost. Furthermore, future works will complement the PWC procedure in order to design fault-tolerant control systems. Finally, the applicability of parallel computing techniques will be analyzed to accelerate the dynamic simulations.

Acknowledgements

The authors would like to express their gratitude to the financial support of CONICET (Consejo Nacional de Investigaciones Científicas y Técnicas), ANPCYT (Agencia Nacional de Promoción Científica y Técnica) and UNR (PRH 24-Subproject 3) and UTN-FRRo from Argentina. The authors also acknowledge the support of professor Francis Doyle, who provided the pulp mill benchmark problem software.

Appendix A. Niederlinski index

Let \tilde{G}_s denote the matrix obtained by setting to zero all elements of G_s that do not correspond to input–output pairings. Thus, $\det(\tilde{G}_s)$ is equal to the product of the nonzero elements.

The Niederlinski index (*NI*) associated to the control structure defined by \tilde{G}_s is (Chiu & Arkun, 1990):

$$NI = \frac{\det[G_s(0)]}{\prod_{P_s} g_s(0)} \quad (22)$$

where P_s represents the set of input–output pairings.

If the *NI* results negative, then the overall structure becomes unstable for a controller with integral term whatever the tuning of the controllers.

Appendix B. Branch and bound comparison

The efficiency of the branch and bound (BAB) approach from Kariwala and Cao (2010) was examined on the pulp mill benchmark problem ($n=57$). This test was carried out on a desktop computer with Intel Pentium Dual-Core E2500 (2.50 Ghz, 4 Gb RAM) using Matlab r2009b.

Table 9

Pareto-optimal set for the pulp mill process.

	BAB solution 1	BAB solution 2
$\mu - IM$	6.32	11.682
RGA-sum	666.49	659.135

Table 10

NRGA-HA and BAB solutions comparison.

	NRGA-HA solution	BAB solution 2
<i>NI</i> index	>0	>0
OPM index	48.899	48.175
$\mu - IM$	12.886	11.682
RGA-sum	660.061	659.135

From the empirical relationship (Eq. (20)) in Kariwala and Cao (2010), the estimated average computation time results 2.17×10^{54} s, which is intractable. However, a computation time limit of 5640 min (4 days) was configured, knowing that only some solutions of the Pareto-optimal set would be obtained (Table 9):

On the other hand, the presented NRGA-HA solution (Section 3.6) was obtained in 0.125 s with the same computer. Comparing this solution with the BAB solution 2 (see Table 10), they only differ in 4 of the 57 pairings. The NRGA-HA solution suggests the pairs: CV37–MV40, CV40–MV5, CV43–MV3 and CV106–MV16. While the BAB solution 2 proposes: CV37–MV5, CV40–MV3, CV43–MV16 and CV106–MV40. The remaining 53 pairs result the same for both solutions.

Both methodologies produce similar solutions (see Table 10), however the NRGA-HA algorithm results computationally efficient for large-scale systems.

Appendix C. Pulp mill model considerations

Inspecting the Simulink model of the benchmark Doyle (2002) it is noted that:

- 1 The Digester Kappa no. (fast) (CV4), and the Digester Kappa no. (slow) (CV5) correspond to the same variable.
- 2 The WL flow to the oxygen tower (which corresponds to the Oxygen Kappa control output) is not declared as a manipulated variable, unlike other Kappa control outputs (i.e. MV20, MV23, and MV26). It is considered as an internal variable in the Simulink model.

According to this, the following actions are taken:

- 1 Only the Digester Kappa no. (slow) (CV5) is considered in the present analysis.
- 2 The white liquor flow to the oxygen tower is considered as a new manipulated variable (it is defined as MV83). This will allow to replace the original Oxygen Kappa control by a PI control (like with MV20, MV23, and MV26). In addition, the Simulink block *WL_fractions1* determines its outputs MV59 and MV49 through algebraic operations based on its inputs MV1, MV2, MV3 (and now also MV83). For this reason, MV59, MV49, and CV101 (which is paired with MV49) will be considered as internal model variables in the present analysis.

Appendix D. G matrix analysis

First, it is necessary to check that all n columns of G are linearly independent so as to avoid $\det(G_s)=0$. Otherwise, all GA solutions will be unfeasible. It is noted that the G columns corresponding to MV48, MV53 and MV73 to MV80 are equivalent. The same happens with the columns associated with MV14 and MV15, and also with

MV19 and MV24. For this purpose, it is decided to consider only one manipulated variable of each of these groups (for instance MV53, MV14 and MV19), and remove the others.

On the other hand, those rows of G which are linear combination of other rows, and also those rows which elements are all zero must be removed. It is noted that the G rows corresponding to CV8 and CV39, CV9 and CV40, CV68 and CV69, CV80 and CV81, CV104 and CV61, CV107 CV109 and CV111, CV108 CV110 and CV112, are respectively equivalent. Then it is decided to consider only one measurement of each of these groups (for instance CV39, CV40, CV69, CV81, CV61, CV111 and CV112), and remove the others. Additionally, the rows corresponding to CV58, CV64 and CV71 are null. Therefore, they are not taken into account.

Finally, it is possible to exclude some MVs such that the maximum RGA-element decreases by several orders of magnitude, as in Castro and Doyle (2002). Applying sequentially this criterion, it is decided to exclude MV27, MV31, MV32, MV34, MV35 and MV57. As a result, the condition number of the filtered G matrix is sensibly reduced. Note that a large condition number could mean that the process has large RGA-elements, which indicates control problems (Skogestad & Postlethwaite, 2005).

Appendix E.

Tables 11 and 12

Table 11
Controller parameters. Fiber line control loops.

CV no.	MV no.	K_c	T_i
3	1	0.01	44
5	2	-0.01	190.2
7	7	-0.02	50
12	6	0.005	-
14	8	1.132	2.5
15	4	0.755	2.5
17	10	0.02	2.2
18	11	0.09	2.2
19	37	-0.03	314.4
20	14	0.05	1
21	17	0.05	120
22	20	-0.46	45
23	22	1.5	3
24	23	0.03	57.4
25	25	1.5	3
26	26	0.03	85.5
28	9	1	9.2
29	33	-0.05	13
30	72	0.13	13
31	21	0.02	2.5
32	30	0.04	13
33	28	0.06	-
35	36	-3.436	20
36	29	-0.069	1
37	40	0.005	-
40	5	0.02	90

Table 12
Controller parameters. Chemical recovery control loops.

CV no.	MV no.	K_c	T_i
41	12	0.1	-
43	3	0.02	-
44	43	0.37	42.5
49	44	-0.1	-
50	42	-0.2	9.2
52	39	-0.19	99.3
56	45	0.2	-
59	47	-0.15	44
60	50	-5	30
61	41	-1	-
62	52	0.1	30.3

Table 12 (Continued)

CV no.	MV no.	K_c	T_i
63	82	-0.18	2.5
72	56	-1	44
75	83	-0.005	-
76	65	0.0001	-
77	70	-0.004	-
78	53	-0.005	-
79	69	0.05	5
81	71	-0.0018	79
82	55	-0.8	30
86	13	0.0015	-
91	51	0.2	22
92	67	0.2	20
93	68	0.21	20
96	66	-0.0035	2.5
98	64	0.0035	500
99	19	0.04	500
106	16	0.05	500
112	58	0.1	-
113	61	0.004	-
114	54	0.1	500

Appendix F.

Tables 13–18

Table 13
Fiber line outputs.

Output no.	Description	Output no.	Description
1	Digester production rate	17–18	Recycle stream no. 1–2
2	Storage production rate	19–20	O Kappa no. and T
3	D_2 production rate	21	D_1 T
4	Digester Kappa no. (fast)	22–23	E Kappa no. and T
5	Digester Kappa no. (slow)	24	E washer $[OH^-]$
6	Digester pulp yield (calculated)	25–26	D_2 T and brightness
7	Bleached pulp yield (calculated)	27–33	Washer no. 1–7 DF
8	Upper extract EA	34	Storage V
9	Lower extract EA	35	O washer effluent T
10	Upper extract conductivity	36	O washer inlet consistency
11	Lower extract conductivity	37	O P
12–14	Cooking T (cook, mcc, emcc)	38	D_2 V
15	Digester WL T	39	Upper extract EA (estimated)
16	Upper extract T	40	Lower extract EA (estimated)

Table 14
Fiber line manipulated variables.

MV no.	Description	MV no.	Description
1	Wood chips flow	19–20	D_1 water and ClO_2 flow
2–3	Dig. WL flow (cook/wash zones)	21–22	E wash water and steam flow
4–8	Dig. steam flows 1–5	23–24	E caustic and water flow
9	Mill water flow	25	E steam flow
10–11	Pulp washing split fraction 1–2	26–27	D_2 ClO_2 and caustic flow
12	O caustic flow	28	D_2 wash water flow
13	Excess WL split fraction	29	O split fraction 2
14–15	O steam flow 1–2	30	E split fraction
16	O split fraction 1	31–35	Pulp washing split fraction 3–7
17	O steam flow 3	36–37	O coolant and oxygen flow
18	Pulp flow to bleach plant	38	Bleached pulp flow

Table 15
Fiber line disturbance variables.

DV no.	Description	DV no.	Description
1–8	Wood chips T and densities	15–16	E caustic T and concentration
9	Mill water T	17	E water stream T
10–11	O caustic T and concentration	18–19	$D_2 \text{ ClO}_2 \text{ T}$ and concentration
12	D_1 mill water T	20–21	D_2 caustic T and concentration
13–14	$D_1 \text{ ClO}_2 \text{ T}$ and concentration	22	D2 wash water T

Table 16
Chemical recovery outputs.

Output no.	Description	Output no.	Description
41	WBL flow	82–83	WL T and causticity
42–44	BL T, flow and concentration	84–85	WL NaOH concentration and flow
45–52	Evaporator no. 1–8 V	86–87	WL NaSH concentration and flow
53–54	Sdt V and density	88–89	Edt NaSH concentration and flow
55–56	Sdt condensate T and vapor flow	90	Mud flow
57	Storage tank 1 V	91–93	Filter 1–3 WLR
58–59	Glc upper V and lower density	94–100	Recycle no. 1–7 flows
60–61	GL T and Na_2CO_3 concentration	101	WL flow
62–64	Slaker T, condensate/vapor flow	102–103	GL density and solids concentration
65	Classifier T	104	GL Na_2CO_3 concentration (estimated)
66–67	Causticizer no. 1 T and EA	105	Causticizer 1 conductivity
68	Causticizer no. 2 T	106	Causticizer 1 EA (estimated)
69–70	Causticizer no. 3 T and EA	107	Causticizer 3 conductivity
71–72	Wlc upper V and lower density	108	Causticizer 3 EA (estimated)
73	Mud mixing tank V	109	Wlc liquor conductivity
74	Storage tank no. 2 V	110	Wlc EA (estimated)
75–76	Lime exit T and front end T	111	WL conductivity
77–78	Kiln hot gas T and back end T	112	WL EA (estimated)
79–80	Kiln O ₂ and CaCO ₃ mass fraction	113	Mud Ca(OH) ₂ concentration
81	Kiln CaCO ₃ (slow)	114	Mud Ca(OH) ₂ mass flow

Table 17
Chemical recovery manipulated variables.

MV no.	Description	MV no.	Description
39	Weak BL split fraction 1	57	Clarified WL flow
40	Evaps. caustic flow 1	58	Caustic make-up flow
41	Evaps. salt-cake flow	59	O WL flow
42–44	Evaps. effects 1–3 steam flow	60	Limemud mixer exit flow
45	Sdt scrubber caustic flow	61	Mud washer filtrate flow
46	Sdt green liquor flow	62	Weak wash make-up water flow
47–48	Glc dregs/clarified liq. flows	63	Limemud flow to filter
49	Green liquor flow to slaker	64	Limemud dilution water flow
50	GL cooler coolant flow	65–66	Limemud split fraction 1–2
51	Dregs filter wash water flow	67–68	Mud filters wash water flow

Table 17 (Continued)

MV no.	Description	MV no.	Description
52	GL split fraction	69–70	Kiln primary/secondary air flow
53	Fresh lime screw speed	71	Kiln fuel flow
54	Lime feed split fraction	72	O wash water flow
55	WL cooler coolant flow	73–80	Effect 8–1 exit flow
56	Wlc limemud flow	81–82	Scrubber coolant flows

Table 18
Chemical recovery disturbance variables.

DV no.	Description	DV no.	Description
23–27	Effect 8–4 P	45	Dregs filter DR
28	Evaps. split fraction	46	Dregs filter water stream T
29	Evaps. caustic stream T	47	Fresh lime T
30	Evaps. salt-cake stream T	48	Ambient T
31–32	Evaps. effect 1 steam T and P	49	WL cooler coolant stream T
33	Evaps. effect 1 vapor dome P	50	Caustic make-up stream T
34–35	Evaps. effect 2 steam T and P	51	Wash wash make-up water T
36	Evaps. effect 2 vapor dome P	52	Limemud dilution water T
37	Evaps. flash tank 1 P	53	Mud filter 1 wash water T
38–39	Evaps. effect 3 steam T and P	54	Mud filter 1 DR
40	Evaps. effect 3 vapor dome P	55	Mud filter 2 wash water T
41	Evaps. flash tank 2 P	56	Mud filter 2 DR
42	Split fraction 3	57	Kiln fuel T
43	Sdt scrubber caustic T	58	Lime screw fill factor
44	GL cooler coolant stream T		

References

- Arkun, Y., & Downs, J. (1990). A general method to calculate input-output gains and the relative gain array for integrating processes. *Computers and Chemical Engineering*, 14, 1101–1110.
- Basualdo, M., Feroldi, D., & Outbib, R. (2012). *PEM fuel cells with bio-ethanol processor systems*. Springer-Verlag London Limited.
- Bristol, E. (1966). On a new measure of interaction for multivariable process control. *IEEE Transactions on Automatic Control*, 11(1), 133–134.
- Buckley, P. S. (1964). *Techniques of process control*. New York, USA: Wiley.
- Cao, Y., & Kariwala, V. (2008). Bidirectional branch and bound for controlled variable selection. Part 1. Principles and minimum singular value criterion. *Computers and Chemical Engineering*, (32), 2306–2319.
- Castro, J., & Doyle, F. (2002). Plantwide control of the fiber line in a pulp mill. *Industrial and Engineering Chemistry Research*, 41(5), 1310–1320.
- Castro, J., & Doyle, F. (2004a). A pulp mill benchmark problem for control: Application of plantwide control design. *Journal of Process Control*, 14(3), 329–347.
- Castro, J., & Doyle, F. (2004b). A pulp mill benchmark problem for control: Problem description. *Journal of Process Control*, 14(1), 17–29.
- Chen, R., McAvoy, T., & Zafriou, E. (2004). Plant-wide control system design: Extension to multiple-forcing and multiple-steady-state operation. *Industrial and Engineering Chemistry Research*, 43, 3685–3694.
- Chiu, M., & Arkun, Y. (1990). Decentralized control structure selection based on integrity considerations. *Industrial and Engineering Chemistry Research*, 29, 369–373.
- Cooper, L., & Steinberg, D. (1974). *Methods and applications of linear programming*. Philadelphia, USA: Saunders Company.
- Downs, J., & Skogestad, S. (2011). An industrial and academic perspective on plantwide control. *Annual Reviews in Control*, 35, 99–110.
- Downs, J. J., & Vogel, E. F. (1993). A plant-wide industrial process control problem. *Computers and Chemical Engineering*, 17(3), 245–255.
- Doyle (2002). Pulp mill benchmark. <http://thedoylegroup.org/research/mill/index.html>
- Fatehi, A., & Shariati, A. (2007). Automatic pairing of MIMO plants using normalized RGA. In *Mediterranean conference on control and automation*. Athens: Greece.
- Kariwala, V., & Cao, Y. (2010). Branch and bound method for multiobjective pairing selection. *Automatica*, (46), 932–936.
- Khaki-Sedigh, A., & Moaveni, B. (2009). *Control configuration selection for multivariable plants*. Berlin, Heidelberg: Springer-Verlag.

- Konda, M., Rangaiah, G., & Krishnaswamy, P. (2005). Plantwide control of industrial processes: An integrated framework of simulation and heuristics. *Industrial and Engineering Chemistry Research*, 44, 8300–8313.
- Ljung, L. (1999). *System identification. Theory for the user* (2nd ed.). New Jersey, USA: Prentice Hall PTR.
- Ljung, L. (2002). System identification toolbox. User's guide version 5. The Math Works Inc.
- Luyben, W., Tyreus, B., & Luyben, M. (1998). *Plant-wide process control*. New York, USA: McGraw-Hill.
- McAvoy, T. (1998). A methodology for screening level control structures in plantwide control systems. *Computers and Chemical Engineering*, 22, 1543–1552.
- Molina, G., Zumoffen, D., & Basualdo, M. (2011). Plant-wide control strategy applied to the Tennessee Eastman process at two operating points. *Computers and Chemical Engineering*, (35), 2081–2097.
- Ochoa, S., Wozny, G., & Repke, J. (2010). Plantwide optimizing control of a continuous bioethanol production process. *Journal of Process Control*, 20, 983–998.
- Rivera, D. (1986). Internal model control. PID controller design. *Industrial & Engineering Chemistry Process Design and Development*, 25, 252–265.
- Rivera, D. (2007). Una metodología para la identificación integrada con el diseño de controladores imc-pid. *Revista Iberoamericana de Automática e Informática Industrial*, 4(4), 5–18.
- Sharifzadeh, M., & Thornhill, N. (2012). Optimal selection of control structure using a steady-state inversely controlled process model. *Computers and Chemical Engineering*, (38), 126–138.
- Skogestad, S. (2000). Plant-wide control: The search for the self-optimizing control structure. *Journal of Process Control*, 10, 487–507.
- Skogestad, S. (2004). Control structure design for complete chemical plants. *Computers and Chemical Engineering*, 28, 219–234.
- Skogestad, S., & Postlethwaite, I. (2005). *Multivariable feedback control. Analysis and design*. Chichester, West Sussex, England: John Wiley & Sons.
- Stephanopoulos, G. (1984). *Chemical process control*. Prentice Hall International Series in the Physical and Chemical Engineering Sciences.
- Vasudevan, S., Rangaiah, N., Konda, M., & Tay, W. (2009). Application and evaluation of three methodologies for plantwide control of the styrene monomer plant. *Industrial and Engineering Chemistry Research*, 48, 10941–10961.